JOHANNES GUTENBERG-UNIVERSITÄT MAINZ
Fachbereich Physik
Institut für Physik

AB

CERN-PRE 89-030

MZ-ETAP/89-5
MAY 1989

Observation and Analysis of E Mesons in $\bar{p}p$ Annihilation at Rest in H_2 Gas*

K. D. Duch[1], M. Heel[2], H. Kalinowsky, F. Kayser[3], E. Klempt, B.May
O. Schreiber[4], P. Weidenauer, and M. Ziegler[5]
Institut für Physik, Johannes-Gutenberg-Universität, 6500 Mainz, Germany

D. Bailey[6], S. Barlag[7], J.M. Butler[8], U. Gastaldi[9], R. Landua[9], C. Sabev
CERN, 1211 Genève, Switzerland

W. Dahme[10], F. Feld-Dahme[11], U. Schaefer[12], W.R. Wodrich[1,9]
Sektion Physik, Ludwig-Maximilians-Universität, 8000 München, Germany

J.C. Bizot, B. Delcourt, J. Jeanjean, H. Nguyen
Laboratoire de l'Accélérateur Linéaire, Université de Paris-Sud, 91405 Orsay, France

E.G. Auld, D.A. Axen, K.L. Erdman, B. Howard, R. Howard, B.L. White
Department of Physics, University of British Columbia, Vancouver, B. C., Canada V6T2A6

S. Ahmad, M. Comyn, G.M. Marshall
TRIUMF, Vancouver, B. C., Canada V6T2A3

G. Beer, L.P. Robertson
Department of Physics, University of Victoria, Victoria, B. C., Canada V8W2Y2

M. Botlo[13], C. Laa[14], H. Vonach
Institut für Kernphysik, Universität Wien, 1090 Wien, Austria

C. Amsler, M. Doser[15], J. Riedlberger, U. Straumann[9], P. Truöl
Physik Institut der Universität Zürich, 8001 Zürich, Switzerland

ASTERIX Collaboration

May 19, 1989

* this work comprises part of the thesis of K. D. Duch

[1] present address: Schott Glaswerke, 6500 Mainz/Wiesbaden, Germany
[2] present address: Boehringer, 6507 Ingelheim, Germany
[3] present address: Volkshochschule, 6450 Hanau, Germany
[4] present address: AT+T, 8000 München, Germany
[5] present address: GEI, 6100 Darmstadt, Germany
[6] present address: University of Toronto, Ontario, Canada M5S1A7
[7] present address: Max Planck Institut, 8000 München, Germany
[8] present address: FNAL, Batavia, Illinois, USA 60510
[9] part of this work was done while at Universität Mainz
[10] present address: LeCroy Research Systems, 1211 Genève, Switzerland
[11] present address: CERN, 1211 Genève, Switzerland
[12] present address: DLR, 7000 Stuttgart, Germany
[13] present address: Österreichische Akademie der Wissenschaften, 1050 Wien, Austria
[14] present address: Voest Alpine, 1050 Wien, Austria
[15] present address: KEK, Tsukuba 305, Japan

Abstract

Antiproton–proton annihilation at rest in a gaseous H_2 target at NTP into the final state $\pi^+\pi^-K^\pm\pi^\mp(K^0)_{miss}$ with an undetected K^0 or $\overline{K}^0$ has been investigated. We observe the E(1420) in the invariant mass spectrum $(K^0)_{miss}K^\pm\pi^\mp$ with $M_E = 1413 \pm 8$ MeV/c^2, $\Gamma_E = 62 \pm 16$ MeV/c^2 and find a 3σ evidence for the production of the $f_1(1285)$ (former D meson). The absolute branching ratio of $\overline{p}p \to \pi^+\pi^-E^0$, $E^0 \to K^0_L K^\pm\pi^\mp$ at $(61 \pm 6)\%$ P wave annihilation is $(3 \pm 0.9)\cdot 10^{-4}$ of all annihilations. The observed suppression of the E production from P wave with respect to the S wave together with some simple selection rules suggest that the quantum numbers of the E(1420) are $J^{PC} = 0^{-+}$ and not 1^{++}.

1. Introduction

One of the most striking predictions of the theory of strong interactions is the existence of states which are composed of gluons, called glueballs, and of states which carry at least a certain amount of glue, called hybrids. Several candidates of such exotic matter have been found so far [1], but more experimental information is still required.

Most theories predict that the first excited glueball should have the quantum numbers $J^{PC} = 0^{-+}$ and a mass of about 1400 MeV/c^2 [2–5]. However the experimental situation in this mass range is rather complex. In 1963 a resonance at 1420 MeV/c^2 was found in $\bar{p}p$ annihilation at rest in a H_2 bubble chamber [6]. It was called E meson. The analysis of the decay Dalitz plot lead to a spin–parity $J^{PC} = 0^{-+}$ [7]. In 1980 a particle with a mass of 1440 MeV/c^2 was discovered in radiative J/Ψ decays and named iota [8,9]. A spin–parity analysis also gave $J^{PC} = 0^{-+}$. Other experiments observed a particle in this mass range partly with quantum numbers $J^{PC} = 1^{++}$ partly with 0^{-+} [10–16]. In γ–γ collisions, in which one photon is highly virtual, a 1^{++} resonance at 1420 MeV was observed [17–20]. Also the width of the resonance varied from experiment to experiment. Therefore the question arose whether there is more than one particle in this mass region. In addition the decay modes support the hypothesis of more than one particle. The resonance was mainly observed in the $K\bar{K}\pi$ channel. Experiments which determined spin and parity to $J^{PC} = 1^{++}$ preferred the decay into $K^*\bar{K}$ + c.c. Those which found $J^{PC} = 0^{-+}$ preferred mostly a decay via $a_0(980)\pi$. However, no clear signal has been seen in the $\eta\pi\pi$ channel [21] although the $a_0(980)$ is mainly observed in the $\eta\pi$ final state.

In this paper we report on a study of E mesons as seen in the ASTERIX detector [22] by stopping antiprotons in a H_2 gas target at normal temperature and pressure (NTP). We call the resonance E meson (even though this name is now mostly used to denote the $f_1(1420)$ meson with $J^{PC} = 1^{++}$) because this is the original name it had been given by the CERN–Collège–de–France Collaboration [6,7] after its discovery in the CERN liquid hydrogen bubble chamber.

The main difference between antiproton annihilations in liquid hydrogen and in gaseous H_2 consists in the angular momentum state of the $\bar{p}p$ system at annihilation. In liquid H_2,

annihilation occurs mainly – due to a mechanism proposed by Day, Snow, and Sucher [23] – from $\bar{p}p$ atomic S states. In gaseous H_2 the DSS mechanism is less effective, and annihilation from S and P states becomes about equally important [24]. When observed in coincidence with an X–ray emitted in a nD → 2P transition (L X–ray), annihilation proceeds with 99% probability from one of the P states [25].

We observe the E in the reaction:

$$\bar{p}p \to \pi^+\pi^- E^0 \to \pi^+\pi^- K^\pm \pi^\mp (K^0)_{miss} \qquad (1)$$

with an unobserved K^0 or $\bar{K}^0$. From the $E^0 \to (K^0)_{miss} K^\pm \pi^\mp$ decay Dalitz plot we find that $K^*\bar{K}$ + c.c. cannot be the dominant decay mode of the E. The branching ratio for production of the E meson is found to be reduced in comparison to the production rate in liquid H_2. Hence reaction (1) is suppressed in P wave annihilations. Simple selection rules then determine the J^{PC} of the resonance to 0^{-+}.

2. Apparatus

The experiment was performed at the Low–Energy Antiproton Ring (LEAR) at CERN using an antiproton beam momentum of 105 MeV/c, the lowest momentum available in 1985 and 1986. The antiprotons were slowed down to rest in a H_2 gas target at normal temperature and pressure.

The general layout of the ASTERIX spectrometer is shown in Fig. 1. The spectrometer consisted of a target and eight cylindrical chambers. They were mounted inside of a solenoidal magnet of 1.4 m length and of 1.8 m diameter. The magnet and some of the chambers (the Q chambers) had been used before at the DCI ring at Orsay [26]. For the present experiment the magnet was extended to house additional chambers. It provided a homogenous magnetic field of 0.8 Tesla. A detailed description of the apparatus and its performance can be found elsewhere [22]. Here we report only on those features which are necessary to understand the analysis presented in this paper.

Antiprotons entered the solenoid along the field axis and were stopped in a cylindrical

gas target positioned in the center of the magnet. Upstream and downstream scintillation counters T2 and T4 inside the gas target were used to define antiproton stops. The target was surrounded by an X–ray Drift chamber (XDC) with cylindrical symmetry and radial electric field (Fig. 2). Target and XDC were separated by a 6 μm thin aluminized mylar foil transparent to X–rays with energies above 1 KeV. The XDC had a geometrical acceptance of 90% of 4π. The signals of X–rays and charged particles were detected on ninety anode wires running parallel to the detector axis. The ionization was sampled in about 40 bins of 32 ns by means of Flash Analogue to Digital Converters (FADC's). For tracks perpendicular to the beam axis each bin contained the ionization of a 1.7 mm track element. The energy loss dE/dx was determined using the "truncated mean" (TM50) of the sample, in which only those dE/dx values are used which are below the mean value of the full sample. The resolution obtained was in agreement with the expected value of $\sigma = 14\%$ for minimum ionizing particles. This resolution suffices to distinguish pions and kaons with momenta below 400 MeV/c (Fig. 3).

Charged particles ionized all along their path and crossed typically four or five drift cells. To distinguish X–rays from charged particles we used the fact that they convert locally; therefore the primary electron cloud was contained in a volume of less than 1 mm^3 and usually drifted to one sense wire. Consequently only one signal wire detected the pulse. A further distinction between X–rays and charged particles is the fast decaying X–ray pulse shape compared to the long pulses of charged particles traversing the XDC.

The fraction of events with a detected low–energy X–ray ($\lesssim 4$ keV) was about 5%. Therefore a special trigger was used to enhance annihilation from P levels. The trigger looked for isolated hits in the XDC requiring charge on one single wire and no charge on adjacent wires. This trigger enriched the fraction of events with a detected low–energy X–ray to 25%. The low–energy X–ray domain shows a prominent signal from the L X–ray series of the $\bar{p}p$ atom plus background contributions. The background in the low–energy range due to bremsstrahlung and argon fluorescence was determined to be $(27 \pm 6)\%$. The method to derive this number is described in detail elsewhere [27]. When antiprotons are stopped in H_2 gas and data are recorded independently of the atomic cascade, the fraction of

P wave annihilation is (52.8 ± 4.8)% [24]. Therefore for four–prong data the fraction of P wave annihilation is (61 ± 6)%. If a low–energy X–ray is explicitly required this fraction increases to (86 ± 4)%.

Target and XDC were surrounded by seven cylindrical multiwire proportional chambers (MWPC's) named (starting from inside) C1, C2, Q1, Q2, P1, Q3, P2. The anode wires ran parallel to the beam axis. Inner and outer cathode surfaces were made of helical wires (Q chambers) or strips (C chambers). The P chambers had anode readout only. The two outermost chambers, Q3 and P2, covered a solid angle of 2π sr.

A fast cluster counting was available on the chambers C1, C2, Q2, and P1. The cluster counting was based on LRS majority logic units (MALU's) developed for this experiment. The number of clusters could be compared to a preset multiplicity for trigger purposes.

Four hits per chamber were required for the data used in the present analysis. One noise hit or one inefficiency was allowed in one of the four chambers.

XDC and MWPC's allowed to track charged particles in the magnetic field. At the maximum field strength the momentum resolution for tracks reaching Q3 is approximately given by:

$$\frac{\sigma_p}{p} = [\,(0.042\,p)^2 + (0.023)^2\,]^{1/2} \quad ,p \text{ in GeV/c} \qquad (2)$$

Gammas, mostly from π^0 and η decays, were detected by conversion in a lead converter with a thickness of 0.9 radiation length. The lead converters were positioned between the chambers P1 and Q3. In addition there were two endcap detectors consisting of three hexagonal multiwire proportional chambers. These chambers had cathode readout on both sides. A lead converter was inserted between the first and the second chamber. The position of the γ conversion point was identified by hits in the two chambers behind the lead foil and no charged track leading to this point. The position sensitive γ detectors cover a solid angle of 3π sr. With the conversion and reconstruction probability of 33%, an overall detection efficiency for γ's of 25% was obtained. The detection efficiency falls sharply for γ energies below 100 MeV. At about 60 MeV the detection efficiency has dropped by a factor of two.

For the present analysis the γ detection is only used to veto on neutral pions in order to get a data sample on reaction (1) with lower background for the spin–parity analysis. It is not used for the determination of the absolute branching ratio.

3. Data Selection

The reaction $\bar{p}p \to \pi^+\pi^- E^0$, $E^0 \to K\bar{K}\pi$, can be studied in different final states by selecting one of the following kaonic decay modes of the E:

$$E \to K_s^0 K^\pm \pi^\mp \quad (3a)$$

$$E \to K_s^0 K_s^0 \pi^0 \quad (3b)$$

$$E \to K^+ K^- \pi^0 \quad (3c)$$

$$E \to (K^0)_{miss} K^\pm \pi^\mp \quad (3d)$$

The reactions 3a,b,c allow the identification of both kaons, and the background rejection is correspondingly easier. The decay modes 3a,b lead to final states with six charge particles. Hence these reactions are not very well suited for a detector which covers only a solid angle of 60% of 4π. The investigation of the decay mode $E \to K^+K^-\pi^0$ is rather complex due to large reflections from the reactions $\bar{p}p \to \omega K^+K^-$ and ηK^+K^-. Therefore we chose reaction 3d for the present analysis.

The analysis is based on about $2 \cdot 10^6$ events. The selection criteria in the first step were: four charged particles with the total charge zero and all tracks reaching at least the P1 chamber. The X–ray enhancing trigger was used for most (95%) of the data taken in October 1985 and June 1986.

Annihilations with pions only in the final state occur more frequently than annihilations in which kaons are produced. Hence the charged kaons have to be identified against an overwhelming background. Therefore we present this part of the data selection in some detail.

The dE/dx measurements in the XDC were calibrated run by run using the energy loss distribution of minimum ionizing pions. The K/π separation was studied by use of the

reaction:

$$\bar{p}p \to \pi^+\pi^-K^+K^- \qquad (4)$$

This final state can be identified using only kinematical cuts. We ask for events with a total momentum of less than 100 MeV/c and a total energy under the four pion hypothesis of less than 1.6 GeV/c^2. In addition we reject events with a probability of more than 1% that all four dE/dx measurements are compatible with pions.

Fig. 3 shows the dE/dx distribution of the events of reaction (4). The pion and kaon bands are clearly visible. In reaction (4) selected events have two kaons and two pions, and the identification of the particles is very easy. For the selection of reaction (1) there are no unambiguous kinematical cuts. Therefore we have to apply stringent cuts on the dE/dx. The dE/dx region chosen to identify kaons for the present data set is shown by the solid line in Fig. 3. From the fraction of accepted events the kaon identification probability d_K can be determined. It is plotted in Fig. 4. The momentum range for which the dE/dx information can be used is limited, but it includes nearly the full phase space for reaction (1). If reaction (1) would proceed via phase space only, the charged kaon momentum would follow the distribution shown as dashed curve in Fig. 4. For this kaon momentum distribution the average loss of events due to the dE/dx cut is about 17%. The momentum distribution of the K_S^0 in reaction (1) but with an observed K_S^0 decay is known from the experiment of ref. [6,7]. The fraction of K_S^0's with a momentum $p \geq 400$ MeV/c is (5–10)%. Hence a momentum cut at 400 MeV/c does not introduce a bias which cannot safely be accounted for by Monte Carlo.

In addition to the dE/dx cut we reject events which pass a kinematical fit to the $\pi^+\pi^-\pi^+\pi^-$ or $\pi^+\pi^-\pi^+\pi^-\pi^0$ hypothesis and events with one or more γ's detected. Background events stemming from the reaction $\bar{p}p \to \pi^+\pi^-\pi^+\pi^-(n\pi^0)$, $n \geq 2$, are suppressed by vetoing on detected γ's. For two π^0 (4 γ) events, the chance of not detecting any γ is $(1-\eta_\gamma)^4 = 0.31$, assuming an average γ detection efficiency $\eta_\gamma = 25\%$. This cut improves the signal–to–background ratio considerably, but also reduces the number of good events,

because 25% of the missing neutral kaons are K^0_S decaying into $\pi^0\pi^0$ and hence suffer from the same reduction factor leading to a reduction of the signal by 18%.

Fig. 5 shows the missing mass squared distribution of the $(K^\pm\pi^\mp\pi^+\pi^-)$ system after these cuts. The peak at $MM^2 \approx 0$ is ascribed to $\pi^0(K^\pm\pi^\mp\pi^+\pi^-)$ events in which two pions stem from a K^0_S decay, the peak at $MM^2 \approx 0.25$ is the missing K^0 signal originating from annihilations into the final state $(K^0)_{miss}K^\pm\pi^\mp\pi^+\pi^-$. The continuum reflects the residual contributions from $\pi^+\pi^-\pi^+\pi^-(n\pi^0)$ events. The events in the hatched area in Fig. 5 are submitted to a kinematical fit to the $(K^0)_{miss}K^\pm\pi^\mp\pi^+\pi^-$ hypothesis. There are 700 events with a confidence level of more than 1%. By kinematical fits to the side bins of the $(K^0)_{miss}$ we find that there are 500 ± 30 signal events and 200 ± 30 background events. The features of the background can be determined from events with low confidence level under the $(K^0)_{miss}K^\pm\pi^\mp\pi^+\pi^-$ hypothesis and by studying the side bins of the $(K^0)_{miss}$ signal in Fig. 5. This background is subtracted in the mass spectra presented in the next sections.

4. Production of E Mesons

Fig. 6 shows the $K^\pm(K^0)_{miss}\pi^\mp$ invariant mass distribution of the final data sample. We use in the following $(K^0)_{miss}$ and ($\overline{K}^0 = \overline{K}^0$ or K^0) as equivalent expressions. There are two entries per event since there are two identical charged pions in the final state. One pion is associated with the neutral $K^\pm(K^0)_{miss}\pi^\mp$ system, the other pion is associated with its production. The latter pion leads to a "wrong" $K\overline{K}\pi$ combination. Charge invariance implies that the two charged pions in $\bar{p}p \to \pi^+\pi^-E^0$ production have the same characteristics. Hence the "wrong" $K\overline{K}\pi$ combination must have the same characteristics as the double–charged $K^\pm(K^0)_{miss}\pi^\pm$ combination (shaded area in Fig. 6). By subtraction of the shaded area one gets Fig. 7, now with one entry per event. The spectrum was fitted by two resonances, described by a convolution of a relativistic Breit–Wigner function and a Gaussian function. The latter describes the experimental resolution of $\sigma = 10$ MeV/c^2 in this mass region. No nonresonant contribution was needed to fit the data. The results of the fit are:

$$M_E = 1413 \pm 8 \text{ MeV}/c^2 \qquad (5a)$$

$$\Gamma_E = 62 \pm 16 \ \text{MeV}/c^2$$

$$M_D = 1282 \pm 20 \ \text{MeV}/c^2 \qquad (5b)$$
$$\Gamma_D < 30 \quad \text{MeV}/c^2$$

The absolute branching ratio for E meson production and decay into $K_L^0 K^{\pm}\pi^{\mp}$ is determined via the relation:

$$B = \frac{N_E}{N_{\bar{p}p} \cdot D_E} \qquad (6)$$

where N_E is the number of selected events, $N_{\bar{p}p}$ the number of $\bar{p}p$ annihilations and D_E is the detection efficiency. Note that N_E refers to the number of E mesons decaying into $K_L^0 K^{\pm}\pi^{\mp}$. In order to determine N_E we take out the veto on γ's and correct for the number of $K_S^0 K^{\pm}\pi^{\mp}$ events. The number of E mesons decaying into $K_L^0 K^{\pm}\pi^{\mp}$ and $K_S^0 K^{\pm}\pi^{\mp}$ are, of course, identical. Since we trigger on events with four charged particles we calculate the branching ratio with respect to all four–prong events. The fraction of four–prong events

$$f_{4pr} = \frac{N_{4pr}}{D_{4pr} \cdot N_{\bar{p}p}} \qquad (7)$$

was determined using data without multiplicity trigger. A value of $f_{4pr} = 0.49 \pm 0.04$ was found. In comparison, the bubble chamber data gave $f_{4pr} = 0.473 \pm 0.030$. By introducing the kaon acceptance d_k we can rewrite (6) in the form:

$$B = \frac{N_E}{N_{4pr}} \cdot \frac{D_{4pr}}{D_E} \cdot f_{4pr} \qquad (8)$$

From the analysis of the mass spectrum in Fig. 7 we determined the percentage of the E signal in this final state to be $(84 \pm 16)\%$. Further we apply a factor to correct for

contributions from $K^0_s \to \pi^0\pi^0$ decays:

$$\frac{f(K^0_L \text{ unseen})}{f(K^0_L \text{ unseen}) + f(K^0_s \to \pi^0\pi^0)} = 0.762 \qquad (9)$$

$f(K^0_L \text{ unseen}) + f(K^0_s \to \pi^0\pi^0) = f((K^0)_{miss})$, since nearly all K^0_L decays are outside our detector. A fit of the $(K^\pm\pi^\mp\pi^+\pi^-)$ missing mass spectrum without the veto on γ's with a Gaussian for the signal of the missing K^0 and a polynominal to describe the background leads to 885 ± 62 $\pi^+\pi^-K^\pm\pi^\mp(K^0)_{miss}$ events. With (9) we find the total number of E mesons decaying into $K^0_L K^\pm\pi^\mp$:

$$N_E = (885 \pm 64) \cdot (0.762) \cdot (0.84 \pm 0.16) = 566 \pm 90 \qquad (10)$$

The detection efficiency of kaons due to the cut described in section 3 depends on the kaon momentum distribution. To determine this value we assume three possibilities: phase space decay of the E meson, decay via $K^*\overline{K}$ + c.c. and decay via $a_0(980)\pi$, both for the hypothesis $J^P = 0^-$ and 1^+. We find:

$$d_k = 0.88 \pm 0.12, \qquad (11)$$

where the error covers the three E decay hypotheses.

The last number to be determined is the relative acceptance of the detector for $\bar{p}p \to \pi^+\pi^-E^0$, $E^0 \to (K^0)_{miss}K^\pm\pi^\mp$ events and for pionic events with four charged tracks. Low momentum kaons have a reduced detection efficiency because of their decay probability, an increased multiple scattering, a momentum cut at 100 MeV/c due to the multiplicity trigger and the dE/dx cuts. Monte Carlo events of the main contributions to the four–prong final state were generated and the following acceptances determined:

$$D(\pi^+\pi^-\pi^+\pi^-) = (5.45 \pm 0.25)\% \qquad (12a)$$

$$D(\pi^+\pi^-\pi^+\pi^-\pi^0) = (5.70 \pm 0.27)\% \quad (12b)$$

$$D(\pi^+\pi^-\pi^+\pi^-\pi^0\pi^0) = (4.47 \pm 0.21)\% \quad (12c)$$

$$D(\pi^+\pi^-E^0) = (3.27 \pm 0.84)\% \quad (12d)$$

The acceptances (a,b,c) were weighted with their relative frequencies [28] and a mean value of $D_{4pr} = (5.2 \pm 0.3)\%$ was found. Hence we have:

$$\frac{D_{4pr}}{D_E} = (1.59 \pm 0.25) \quad (13)$$

Putting all correction factors together we find a branching ratio for $\bar{p}p \to \pi^+\pi^-E^0$, $E^0 \to K_L^0K^\pm\pi^\mp$ of

$$B = (3.0 \pm 0.9)\cdot 10^{-4} \quad (14)$$

Fig. 8 shows the dependence of the absolute branching ratio for $\bar{p}p \to \pi^+\pi^-E^0$, $E^0 \to (K^0)_{miss}K^\pm\pi^\mp$ where $(K^0)_{miss}$ stands for K_S^0 in case of ref.[29] and for K_L^0 in case of this experiment. The branching ratio decreases with increasing fraction of P wave annihilation. The extrapolation to 100% P wave annihilation gives a result compatible with zero. Hence the reaction (1) is suppressed from P states of the $\bar{p}p$ atom. If a low energetic X–ray is required to be detected, the statistics is reduced by a factor of 4.2 and the fraction of P wave annihilation increases from $(61 \pm 6)\%$ to $(86 \pm 4)\%$. When we estimate the number of E and $f_1(1285)$ events under the assumption that the E is only produced in S wave and the $f_1(1285)$ only in P wave, then we expect 62 ± 14 events of the type $\bar{p}p \to \pi^+\pi^-(K^0)_{miss}K^\pm\pi^\mp$ in coincidence with a low energetic X–ray but we observe 87 ± 15 events (from a histogram similar to that of Fig. 5). A simple reduction of the branching ratio by a factor 4.2 would lead to 112 ± 7 events.

Finally we note that the dipion recoiling against the E meson and the E meson are produced with relative angular momentum $L = 0$. This angular momentum can be

determined from the decay angular distribution of the pion of the E decay. The decay angular distribution, shown in Fig. 9, is flat as expected for L = 0. Of course, higher angular momenta are unlikely because of the low recoil energy of the E meson.

Table I lists the angular momentum l between the two recoiling pions and the angular momentum L between dipion and the E meson. Isoscalar pion–pion scattering at very low momenta is dominated by l = 0 [30]. From Fig. 9 we see that the angular momentum L also vanishes. The assumption that both angular momenta l and L vanish gives a natural explanation of the observed selection rule: With l = L = 0, $\pi^+\pi^-E^0$ production is only possible from the $^1S_0$ state and forbidden from P states, if the E has quantum numbers $J^{PC} = 0^{-+}$. On the contrary, l = L =0 lead to suppression of mesons with $J^{PC} = 1^{++}$ from S states while production from P states is allowed. Indeed, the $f_1(1285)$ meson is observed in our data sample (with ≈ 60% P wave annihilation) while it was not observed in bubble chamber experiments (with mostly S wave annihilation).

Further support for this interpretation can be derived from η' production. We observe the η' in the reaction $\bar{p}p \to \pi^+\pi^-\eta'$, $\eta' \to \pi^+\pi^-\gamma$. While the branching ratio for $\bar{p}p \to \pi^+\pi^-\eta'$ was found to be $(3.3 \pm 0.8)\cdot 10^{-3}$ in a bubble chamber [31], we find a branching ratio of $(1.5 \pm 0.7)\cdot 10^{-3}$ from P states of the $\bar{p}p$ atom [32]. In both cases about 50% of the reaction proceeds via $\rho\eta'$, i.e. via $\pi^+\pi^-$ in P wave, but in 50% via $\pi^+\pi^-$ in a relative S state. We have again a suppression of a high–mass pseudo–scalar meson from P states. From these arguments we conclude that the suppression of the E production from atomic P states provides clear evidence that the quantum numbers of the E meson as observed in $\bar{p}p$ annihilation at rest are $J^{PC} = 0^{-+}$ and not 1^{++}.

5. E Decay Dalitz Plot

For further analysis we go back to Fig. 5 and define the E meson by a mass cut of $1.37 \leq M(K\bar{K}\pi) \leq 1.48$ GeV/c^2. The background in this mass range consists of $\pi^+\pi^-\pi^+\pi^-(n\pi^0)$ events {(25 ± 6)%} and of the wrong pion combinations in the $\pi^+\pi^-K^\pm\pi^\mp(K^0)_{miss}$ final state {(12 ± 4)%}. Both background contributions show a $K\bar{K}\pi$ Dalitz plot which is compatible with a Dalitz plot produced by $\bar{p}p \to \pi^+\pi^-K^\pm\pi^\mp(K^0)_{miss}$ Monte Carlo events generated

according to a phase space distribution. Therefore we treat the background as phase space events.

Fig. 10 shows the decay Dalitz plot of the E meson. The boundary curve indicates the kinematically allowed region for events in which the E meson has a mass of less than 1420 MeV/c^2. The only visible structure is an accumulation of events in the upper right part of the plot. There are no visible K^* bands. This can also be seen from the $K\pi$ invariant mass squared distributions. They are shown in Fig. 11a for the neutral $K\pi$ system and in Fig. 11b for the charged combinations (two entries per event). The position of the K^* is marked by an arrow. We are aware of the fact that the K^* might be shifted towards a lower mass due to phase space limitations. But even then the contribution of K^*'s must be small. Fig. 12 shows the $K\overline{K}$ invariant mass squared distribution. There is a significant concentration of events with very low $K\overline{K}$ invariant masses. The shape of the phase space is drawn in as a dotted line.

Mass and width of the E meson, the decay Dalitz plot and its projections are fully compatible with the results obtained 20 years ago by the Collège–de–France collaboration [7]. In that experiment no charged E mesons were observed; hence the isospin $I_E = 0$. The decay mode $E \to K^0_S K^0_S \pi^0$ was seen, but $E \to K^0_S K^0_L \pi^0$ was not. Hence the C parity $C_E = +1$ and the G parity $G_E = +1$ implying $G(K\overline{K}) = -1$. With $I(K\overline{K}) = 1$ we must have even angular momentum between the two kaons. Possible assignments to $J^P(K\overline{K})$ are 0^+, 2^+, ... The accumulation of events at low $K\overline{K}$ masses strongly favours $J^P(E) = 0^-$, 1^+, 2^-, ... Because of the controversary between the two assignments $J^P(E) = 0^-$ and 1^+ we tried these two possibilities to reproduce our experimental Dalitz plot and its projections.

Due to our limited solid angle and limited kaon detection efficiency the acceptance over the $K\overline{K}\pi$ Dalitz plot is not uniform. The acceptance Dalitz plot is constructed using the momenta of Monte Carlo generated events after event reconstruction and all selection cuts. It varies by a factor of up to two in those parts of the plot in which the K^* bands are expected.

The acceptance Dalitz plot is multiplied with a matrix element squared describing the E decay dynamics. We use two intermediate states: $E \to a_0(980)\pi$, $a_0(980) \to K\overline{K}$ and $E \to K^*\overline{K}$,

$K^* \to K\pi$. The K^* is parametrized by a relativistic P wave Breit–Wigner function. Mass and width are taken from the Particle Data Group [33]. For the $K\overline{K}$ threshold effect we use two different parametrizations: a normal Breit–Wigner function with PDG values for mass and width, and a coupled channel Breit–Wigner as derived by Flatté [34]. Due to our limited statistics we do not find any significant differences, and we present results only using the Flatté parametrization.

The acceptance Dalitz plot with uniform weight factors is used to describe the background. The matrix elements of the decay modes via intermediate resonances are constructed according to the Zemach method [35]. The decay matrix elements used for the analysis are presented in Table II. Monte Carlo Dalitz plots are generated by multiplication of the acceptance Dalitz plot with the relevant transition matrix elements. The transition matrix elements are calculated from the Monte Carlo generated momenta.

Fig. 13 shows Monte Carlo Dalitz plots representing E decays into $K^*\overline{K}$ + c.c. or $a_0(980)\pi$ for $J^{PC}(E) = 0^{-+}$ and 1^{++}, respectively. We can fit the experimental Dalitz plot with one of the Dalitz plots of Fig. 13 or with contributions from both, $K^*\overline{K}$ + c.c. and $a_0(980)\pi$. The results of the fits are presented in Table III.

Obviously the statistics is not sufficient to draw definite conclusions on the quantum numbers of the E meson. There is only a slight preference for $J^{PC} = 0^{-+}$ originating from two results of the fit. First, the background is fitted too high for $J^{PC} = 1^{++}$ and second, if both 0^{-+} and 1^{++} amplitudes are offered to the fit, the fit decides for 80% 0^{-+} amplitude and 20% 1^{++} amplitude.

The fit, however, is sensitive to the decay mode of the E. The assumption that the dominant decay mode of the E meson is $K^*\overline{K}$ + c.c. is not consistent with our data. For both J^{PC} assignments the fit accepts only a small fraction of $K^*\overline{K}$ + c.c., while the data are compatible with the assumption that $a_0(980)\pi$ is the most prominent decay mode. It should be pointed out, however, that the decay angular distribution of the $K\overline{K}$ system is not flat (Fig. 14), even after acceptance corrections. The angular distribution shows an enhancement at $\cos\theta_{K\overline{K}} = 0$ which is most easily interpreted as the reflection of K^* bands. Yet in the $(K\pi)$ mass spectrum the K^* is not visible. The fit, however, does not exclude a 20–30%

$K^*\overline{K}$ + c.c. contribution which could be responsible for the bump at $\cos\theta_{K\overline{K}} = 0$. Therefore we do not give definite decay branching ratios for $E \to K^*\overline{K}$ + c.c. and $a_0(980)\pi$ but state only that $K^*\overline{K}$ + c.c. is not the dominant decay mode of the E meson as observed in this experiment in contrast to the E meson produced in other hadronic reactions [11,12].

6. Summary and Conclusions

We have observed 500 events of the type $\bar{p}p \to \pi^+\pi^- E^0$, $E^0 \to (K^0)_{miss} K^\pm \pi^\mp$ by stopping antiprotons in hydrogen gas. In addition a small signal is observed in the same final state which we ascribe to the reaction $\bar{p}p \to \pi^+\pi^- f_1(1285)$. The branching ratio for E production and decay into $K^0_L K^\pm \pi^\mp$ was determined. We find $BR(\pi^+\pi^- E^0, E^0 \to K^0_L K^\pm \pi^\mp) = (3.0 \pm 0.9)\cdot 10^{-4}$ with 60% of the antiprotons annihilating from P states of the $\bar{p}p$ system. The CERN Collège–de–France collaboration had found a branching ratio of $BR(\pi^+\pi^- E^0, E^0 \to K^0_S K^\pm \pi^\mp) = (7.1 \pm 0.35)\cdot 10^{-4}$. In that experiment antiprotons were stopped in liquid H_2 leading to more than 90% annihilations from S wave. No $f_1(1285)$ was seen. From the comparison we conclude that E mesons are produced from S states of the $\bar{p}p$ system only, while $f_1(1285)$ mesons are produced from P states only. The assumption that no angular momenta are involved in these reactions – which is supported by data – implies that high–mass mesons with quantum numbers 0^{-+} are only produced from the $^1S_0$ state and 1^{++} mesons only from the $^3P_1$ state of the $\bar{p}p$ atom. In liquid H_2, the production rates for $\pi^+\pi^- E^0$ are $(2.0 \pm 0.2)\cdot 10^{-3}$ from the $^1S_0$ state and $(0.60 \pm 0.06)\cdot 10^{-3}$ from the $^3S_1$ state [7]. Taking into account the statistical weights of the two S states, the transition probability into $\pi^+\pi^- E^0$ from the $^3S_1$ state is found to be suppressed by a factor of 10 in comparison to the transition probability from the $^1S_0$ state. These arguments lead to quantum numbers of the E meson as produced in $\bar{p}p$ annihilation at rest of 0^{-+} and not 1^{++}.

A spin–parity analysis of the E decay Dalitz plot gave no definite conclusions on the E quantum numbers. However the data show a strong $K\overline{K}$ threshold effect in the E decay. We describe the enhancement by a $a_0(980)$ resonance. We believe that a better understanding of the $K\overline{K}$ threshold effect is required before a satisfactory description of a high statistics E decay Dalitz plot can be obtained. Our data prefer $E \to a_0(980)\pi$ over $K^*\overline{K}$ + c.c., but due to

our limited statistics we give no relative branching ratios for these two decay modes. However our data are incompatible with the assumption of a dominant $K^{*}\overline{K}$ + c.c. decay mode of the E, and prefer dominance of the $a_0(980)\pi$ decay mode.

The support of the LEAR staff during the runs is gratefully acknowledged. This work was supported in part by the Deutsches Bundesministerium für Forschung und Technologie, the French Institut National de Physique Nucléaire et de Physique des Particules, the Schweizer Nationalfonds, the Österreichischer Nationalfonds and the Natural Sciences and Engineering Research Council of Canada.

We appreciate the support of Prof. Č. Zupaničič, and the continuous encouragement and active participation of Dr. R. Armenteros.

REFERENCES

[1] A. Palano, CERN/EP 87–92

[2] Schierholz, DESY Report (1989)

[3] R. Shifman, Nucl. Phys. B147 (1979) 385

[4] C.E. Detar and J.F. Donoghue, Ann. Rev. Nucl. Science 33 (1983) 235

[5] K. Hasenfratz, Physics Reports 40C (1978) 75

[6] R. Armenteros et al., Proc. Sienna Int. Conf. Elem. Part., Vol I (1963) 287

[7] P. Baillon et al., Il Nuovo Cimento 50A (1967) 393
P. Baillon et al., BNL (1983) 78
P. Baillon, CERN/EP 83–82

[8] D.L. Sharre et al., Phys. Lett. B97 (1980) 329

[9] C. Edwards et al., Phys. Rev. Lett. 49 (1982) 259

[10] C. Dionisi et al., Nucl. Phys. B169 (1980) 1

[11] T.A. Armstrong et al., Z. Physik C34 (1987) 23

[12] T.A. Armstrong et al., Phys. Lett. B146 (1984) 273

[13] D.F. Reeves et al., Phys. Rev. D34 (1986) 1960

[14] S.U. Chung et al., Phys. Rev. Lett. 55 (1985) 779

[15] A. Birman et al., Phys. Rev. Lett. 61 (1988) 1557

[16] H. Aihara et al., Phys. Rev. Lett. 57 (1986) 2500

[17] Z. Ajaltouni et al., LAL/85–27

[18] H. Aihara et al., Phys. Rev. D38 (1988) 1

[19] P. Hill et al., Z. Physik C42 (1989) 355

[20] H.J. Behrend et al., Z. Physik C42 (1989) 367

[21] A. Ando et al., Phys. Rev. Lett. 57 (1986) 1296

[22] S. Ahmad et al., The ASTERIX detector, still in preparation

[23] T.B. Day et al., Phys. Rev. 118 (1960) 864

[24] M. Doser et al., Nucl. Phys. A486 (1988) 493

[25] E. Klempt, "Antiprotonic Hydrogen", in: "The Hydrogen Atom", Satellite Meeting of the XI Int. Conf. on Atomic Physics, Pisa, June 1988, Proceedings ed. by F. Bassani, Springer Verlag, Berlin, Heidelberg, New York, Tokyo

[26] A. Cordier et al., Nucl. Instr. Meth. 133 (1976) 237

[27] U. Schaefer al., Nucl. Phys. A, in print

[28] C. Ghesquière, Symp. on $\overline{\text{N}}\text{N}$ Interactions, Liblice, CERN 74–18 436

[29] R. Armenteros and B. French, Academic Press Inc., New York, 1969, vol. 4
ASTERIX proposal, CERN/PSCC/80–101

[30] G. Kernel et al., Phys. Lett. B216 (1989) 244

[31] M. Foster et al., Nucl. Phys. B8 (1968) 174

[32] P. Weidenauer et al., η and η' production in pp annihilation at rest, in preparation

[33] Review of Particle Properties, Phys. Lett. B170 (1986)

[34] S.M. Flatté, Phys. Lett. B63 (1976) 224

[35] C. Zemach, Phys. Rev. B133 (1964) 1201
C. Zemach, Phys. Rev. B140 (1965) 97
C. Zemach, Phys. Rev. B140 (1965) 109

FIGURE CAPTIONS

Fig. 1 Side and front views of the ASTERIX spectrometer. 1 – H_2 gas target, 2 – X–ray drift chamber, 3 – lead converter, 4 – cylindrical MWPC, 5 – coil, 6 – yoke, 7 – planar MWPC.

Fig. 2 Gas target and X–ray Drift Chamber (XDC). 1 – anode signal wires, 2 – field shaping wires, 3 – mylar membrane, 4 – argon/ethane drift volume, 5 – H_2 gas target, T2 – beam defining counter, T3,T4 veto counters.

Fig. 3 Ionisation density of tracks in the central drift chamber (XDC). Annihilations into $\pi^+\pi^-K^+K^-$ were selected. The solid line shows the dE/dx cut used to identify the kaon in the final state $\pi^+\pi^-K^\pm\pi^\mp(K^0)_{miss}$.

Fig. 4 Kaon identification efficiency due to the dE/dx cut shown in Fig. 3. The dotted line shows the kaon momentum distribution assuming phase space for E production and decay.

Fig. 5 Missing mass squared distribution recoiling against the $(K^\pm\pi^\mp\pi^+\pi^-)$ system. The peak at $MM^2 = 0.25$ is assigned to undetected neutral kaons. The events shown in the hatched area are submitted to a kinematical fit.

Fig. 6 $K^\pm(K^0)_{miss}\pi^\mp$ invariant mass distribution. There are two entries per event. The double–charged combination $K^\pm(K^0)_{miss}\pi^\pm$ is also shown (shaded area).

Fig. 7 $K^\pm(K^0)_{miss}\pi^\mp$ mass distribution after subtraction of the $K^\pm(K^0)_{miss}\pi^\pm$ mass distribution. The solid line shows a fit with two Breit–Wigner functions folded with the experimental resolution.

Fig. 8 Branching ratio for $\bar{p}p$ annihilation into $\pi^+\pi^- E^0$ with $E^0 \to K^0_{s,L} K^\pm \pi^\mp$ as a function of the contribution of P wave annihilation.

Fig. 9 Decay angular distribution of the dipion recoiling against the E meson. There are two entries per event. The distribution is flat. The angular distribution of the double–charged ($\pi\pi$) system is also shown.

Fig. 10 E decay Dalitz plot. E mesons are defined by a mass cut from 1.37 to 1.48 GeV/c^2 in Fig. 7. The boundary curve indicates the kinematically allowed region for masses lower than 1.42 GeV/c^2.

Fig. 11 ($K\pi$) invariant mass squared distributions. The positions of the K^* bands are indicated. The fit is described in the text.

Fig. 12 $K\bar{K}$ invariant mass squared distribution. A strong enhancement at threshold is observed. The fit is described in the text.

Fig. 13 Monte Carlo E meson decay Dalitz plots for: a) $1^{++} \to a_0\pi$; b) $0^{-+} \to a_0\pi$; c) $1^{++} \to K^*\bar{K}$; d) $0^{-+} \to K^*\bar{K}$.

Fig. 14 Decay angular distribution of the $K\bar{K}$ system. An enhancement at $\cos\theta_{K\bar{K}} = 0$ is expected if there is significant K^* production ($M^2(K\bar{K}) \lesssim 1.1$ GeV$^2/c^4$).

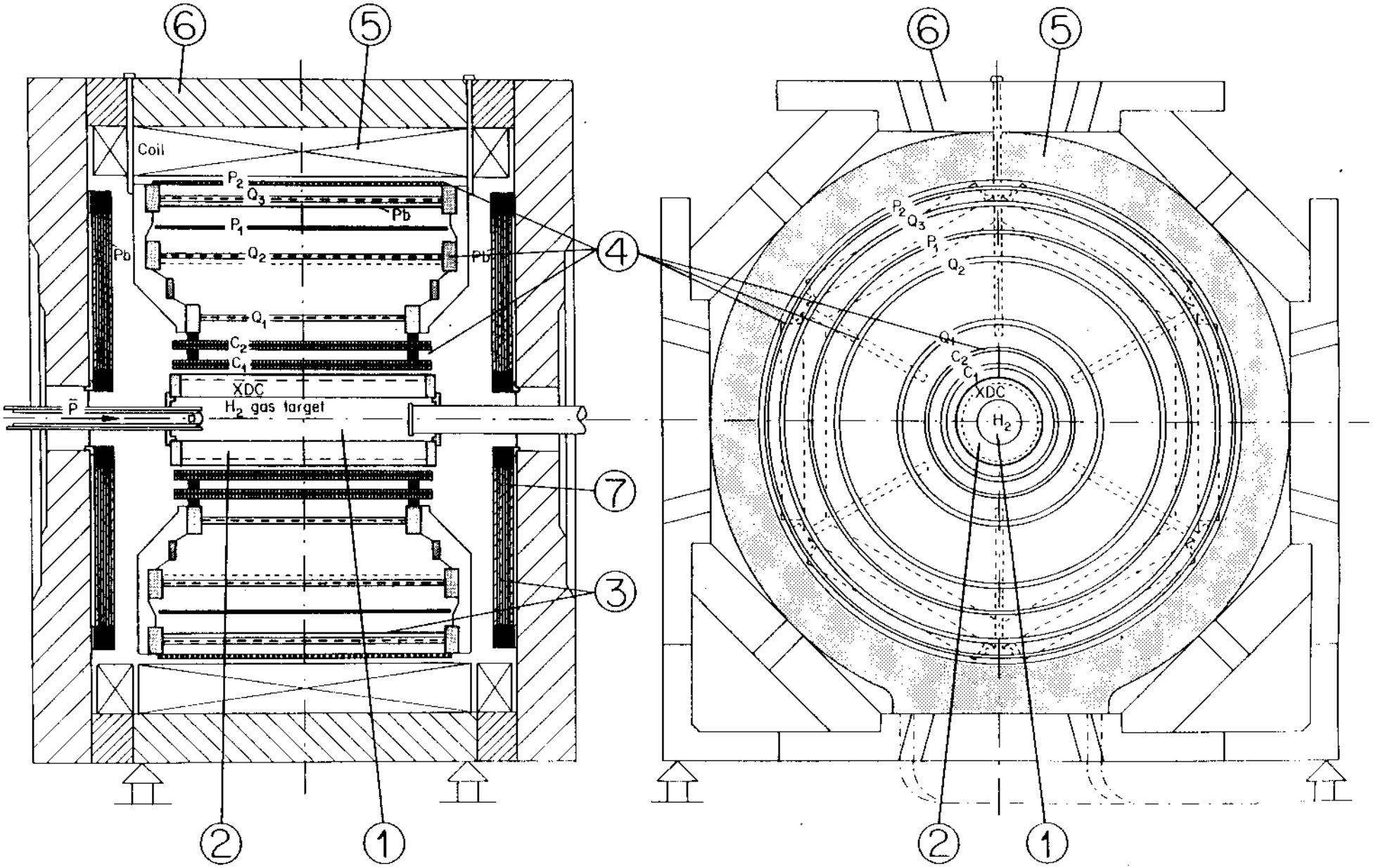
6
5
Coil
P2
Q3
Pb
P1
Q2
Pb
Pb
4
Q1
C2
C1
XDC
H2 gas target
p
7
3
2
1
6
5
P2
Q3
P1
Q2
Q1
C2
C1
XDC
H2
2
1

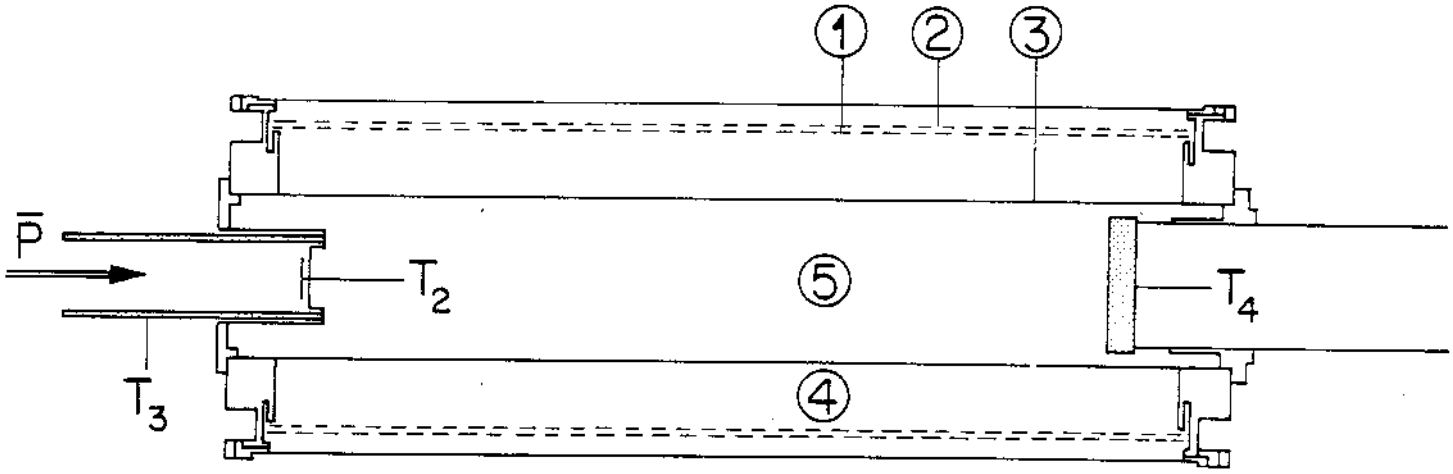
1
2
3
$\bar{P}$
T_2
5
T_4
T_3
4

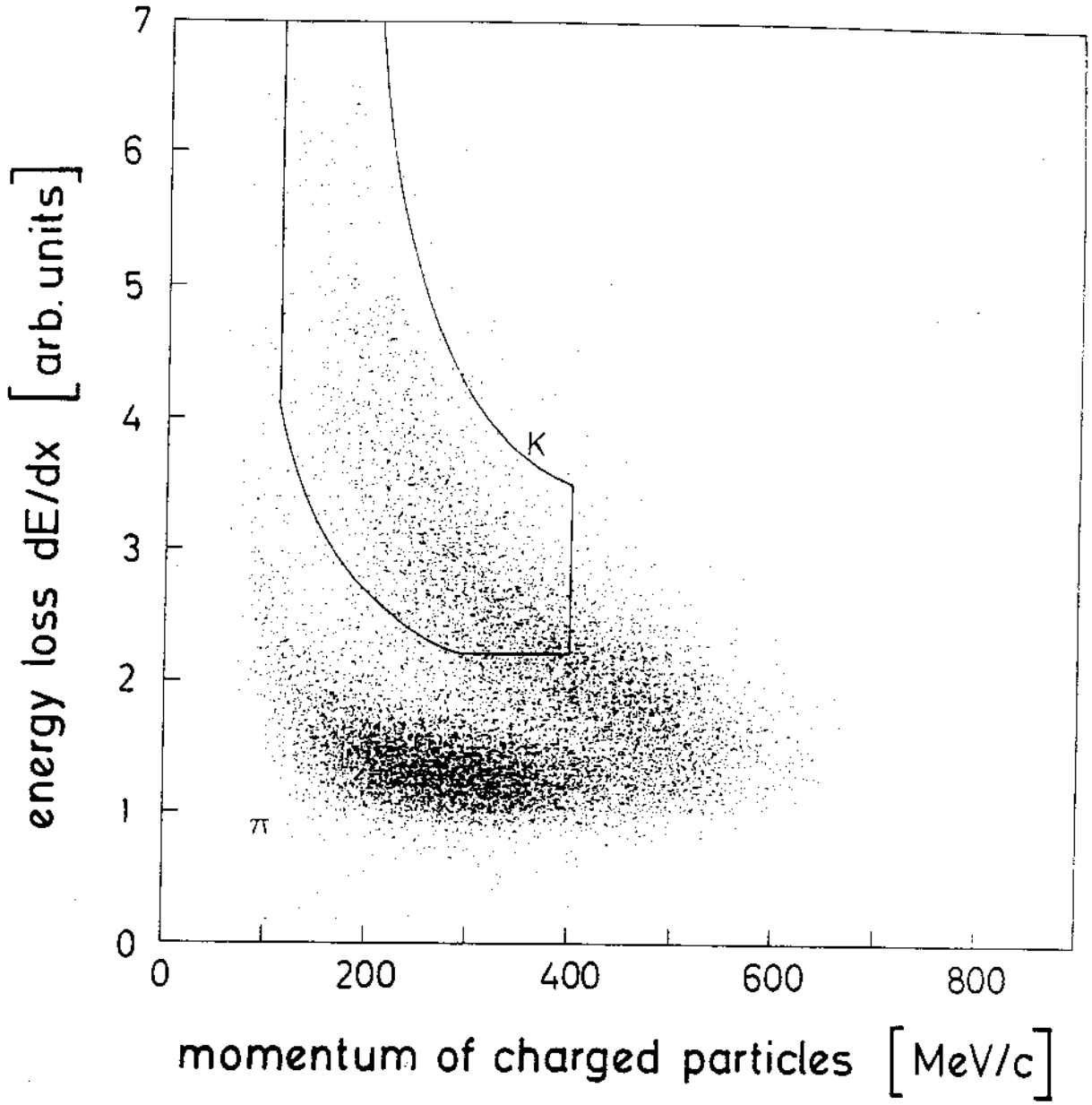
energy loss dE/dx [arb.units]
momentum of charged particles [MeV/c]
K
π
0
1
2
3
4
5
6
7
0
200
400
600
800

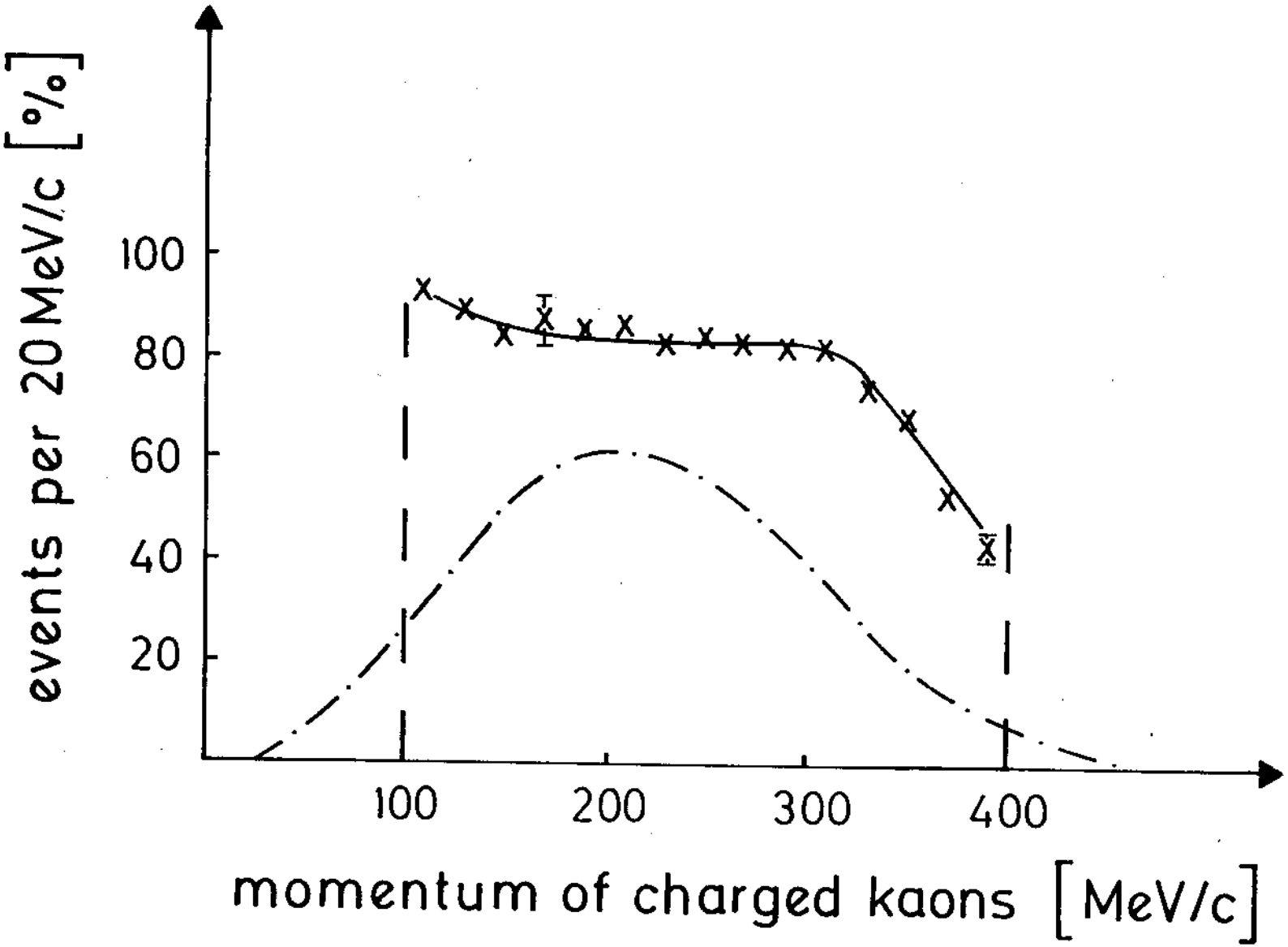
events per 20 MeV/c [%]
100
80
60
40
20
100
200
300
400
momentum of charged kaons [MeV/c]

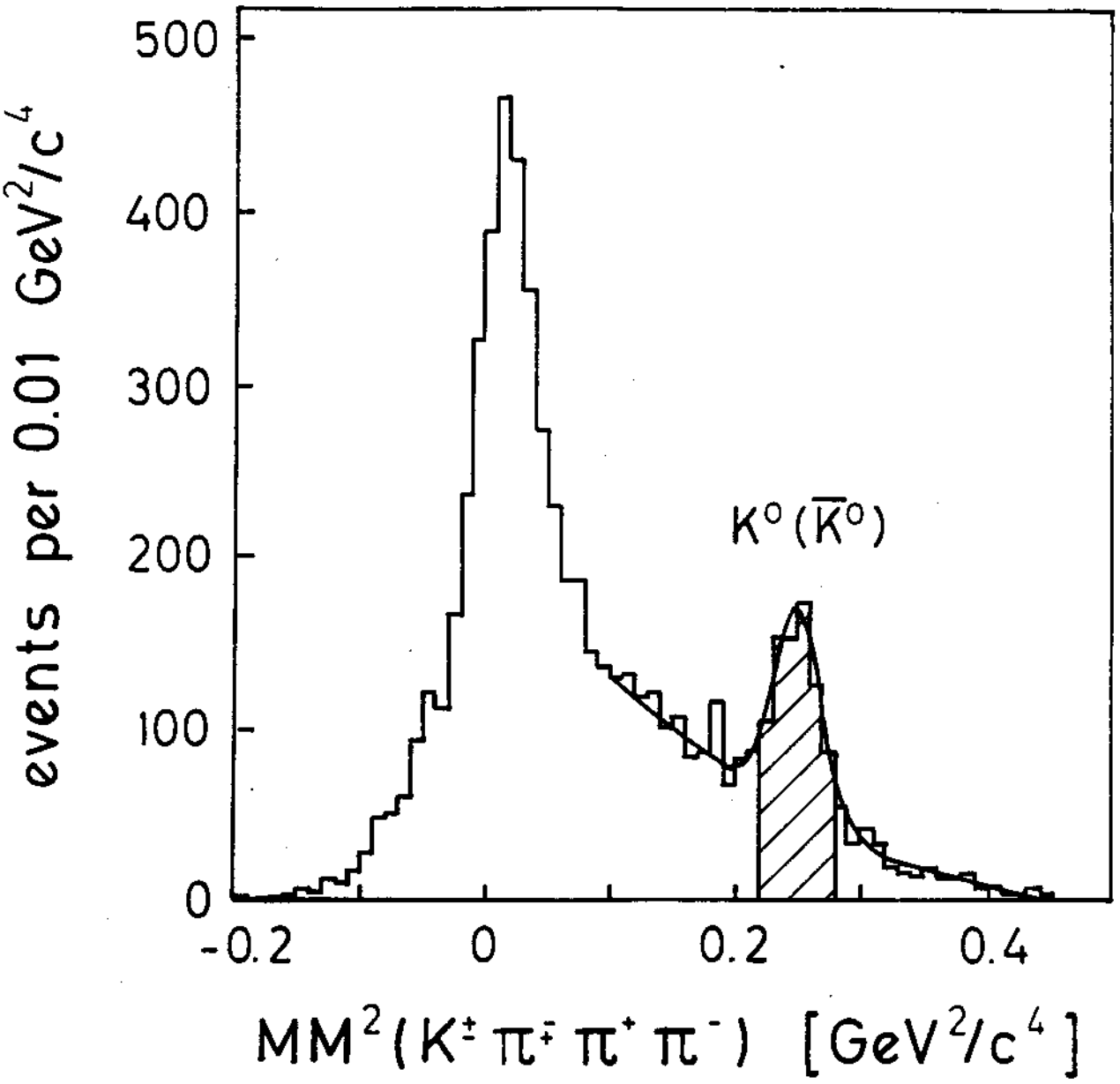
500
400
300
200
100
0
events per 0.01 GeV²/c⁴
K°(K̄°)
-0.2
0
0.2
0.4
MM²(K± π∓ π⁺ π⁻) [GeV²/c⁴]

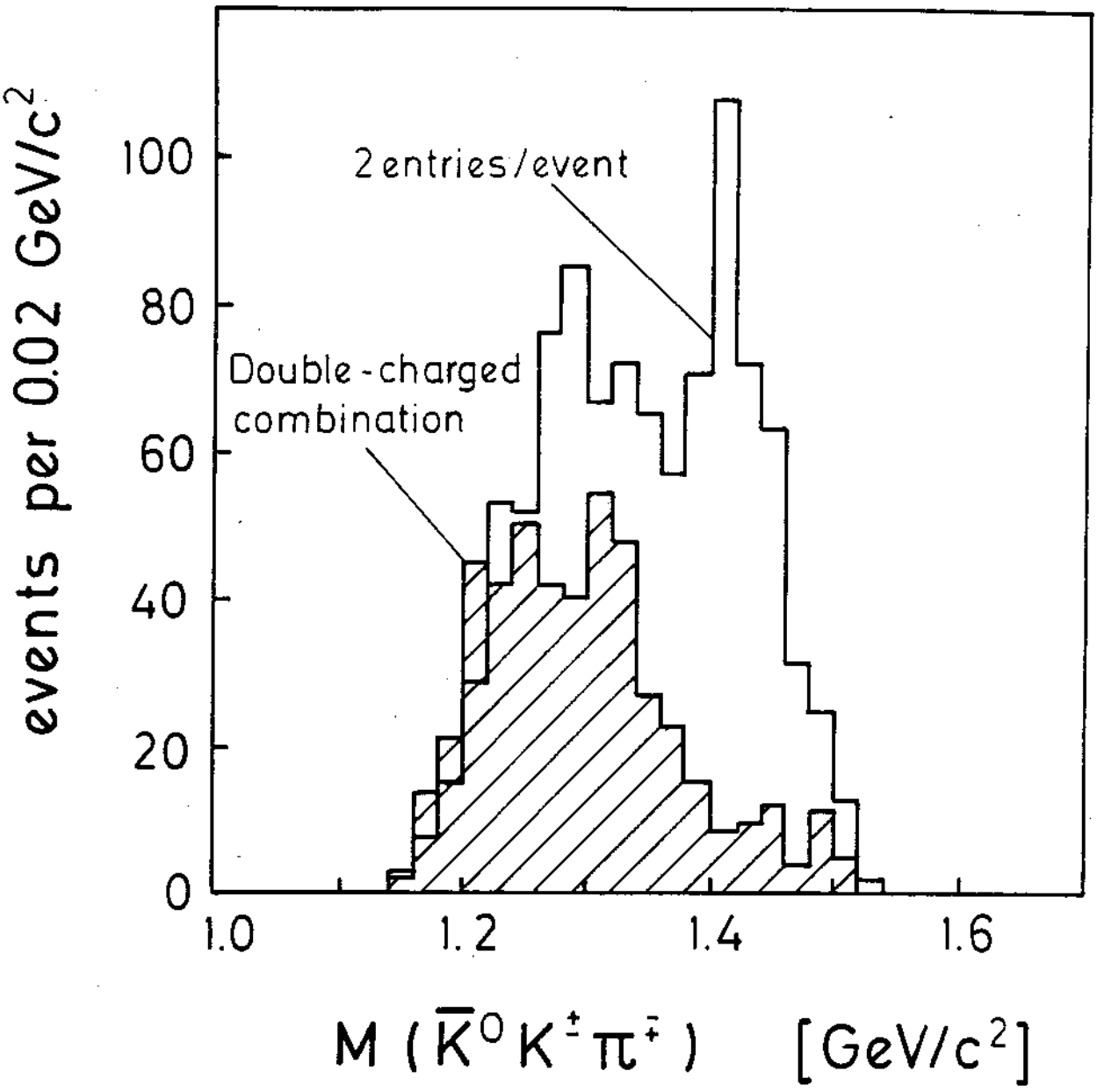
events per 0.02 GeV/c²
100
80
60
40
20
0
2 entries/event
Double-charged
combination
1.0
1.2
1.4
1.6
M ($\bar{K}^0 K^\pm \pi^\mp$) [GeV/c²]

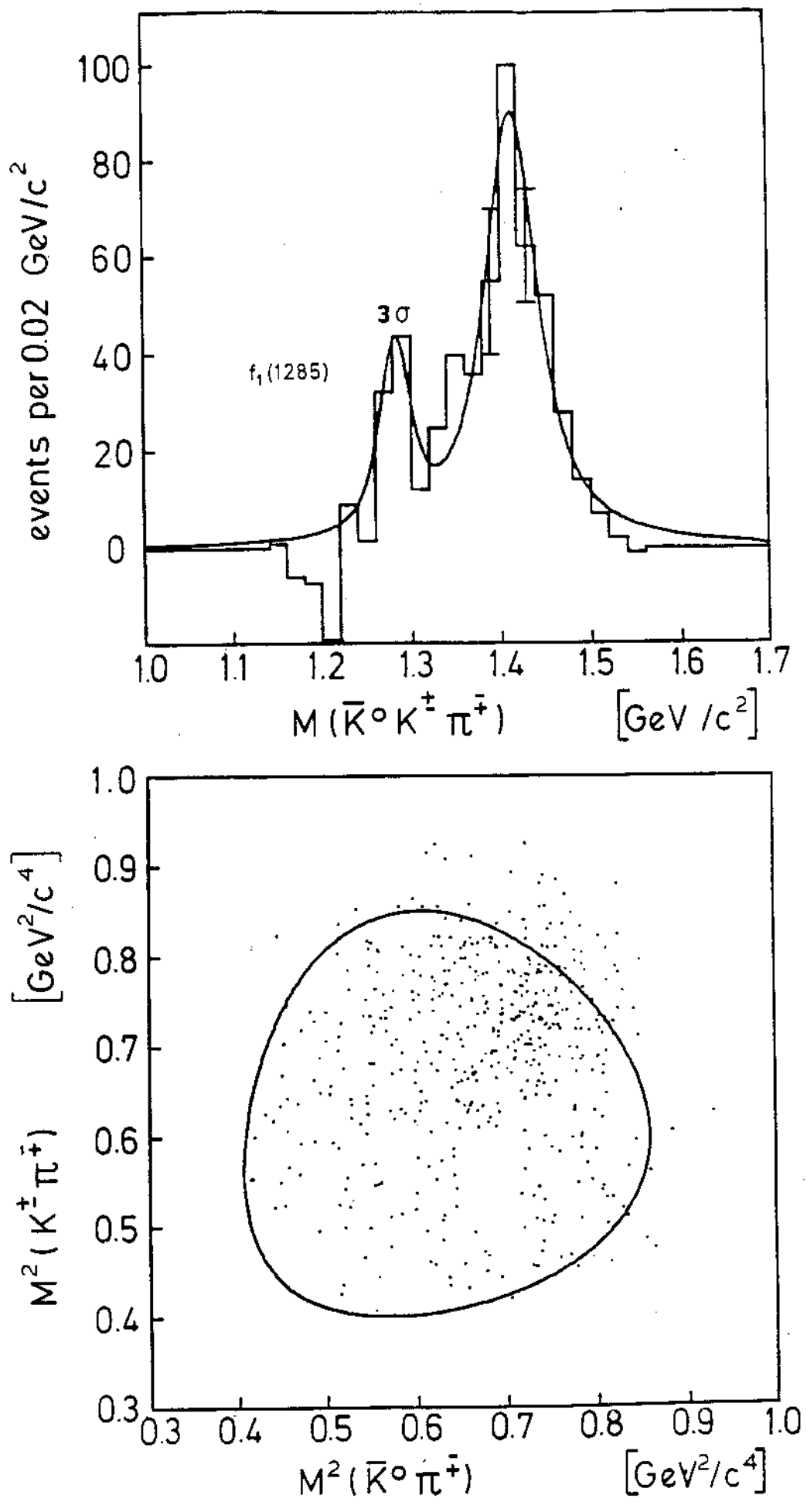
events per 0.02 GeV/c²
100
80
60
40
20
0
3σ
f₁(1285)
1.0
1.1
1.2
1.3
1.4
1.5
1.6
1.7
M (K̄° K± π∓)
[GeV /c²]
M² (K± π∓)
[GeV²/c⁴]
1.0
0.9
0.8
0.7
0.6
0.5
0.4
0.3
0.3
0.4
0.5
0.6
0.7
0.8
0.9
1.0
M² (K̄° π∓)
[GeV²/c⁴]

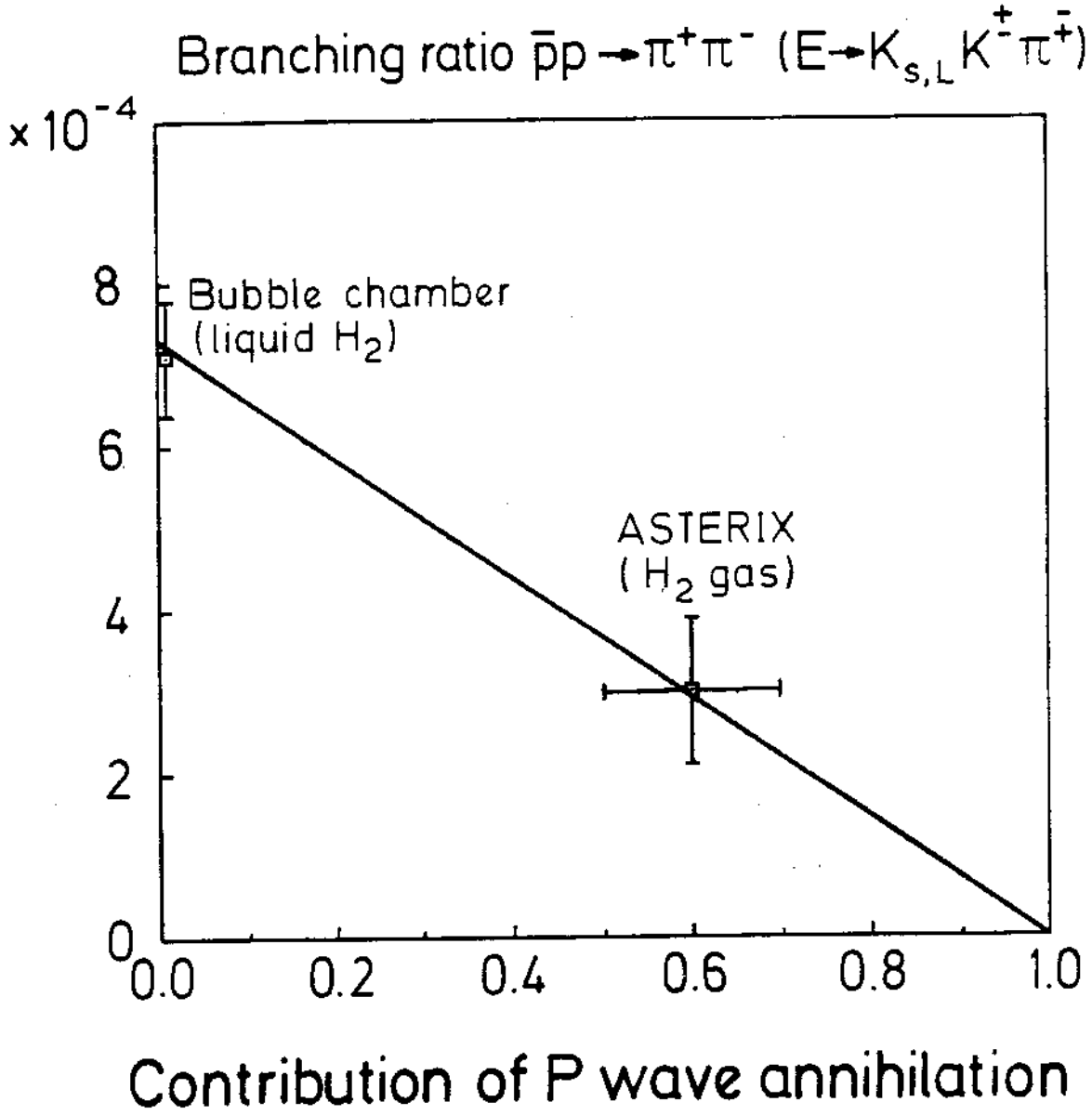
Branching ratio $\bar{p}p \to \pi^+\pi^-$ ($E \to K_{s,L}K^{\pm}\pi^{\mp}$)
$\times 10^{-4}$
8
6
4
2
0
Bubble chamber
(liquid H_2)
ASTERIX
(H_2 gas)
0.0
0.2
0.4
0.6
0.8
1.0
Contribution of P wave annihilation

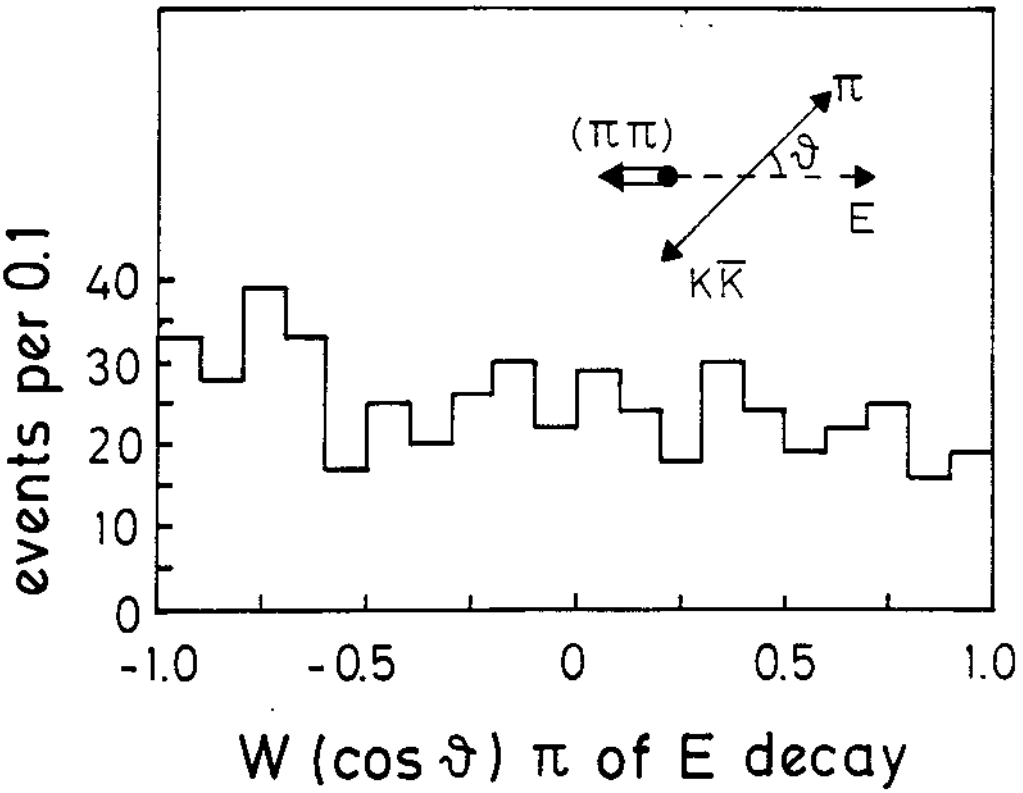
events per 0.1
40
30
20
10
0
-1.0
-0.5
0
0.5
1.0
W (cos ϑ) π of E decay
(ππ)
π
ϑ
E
KK̄

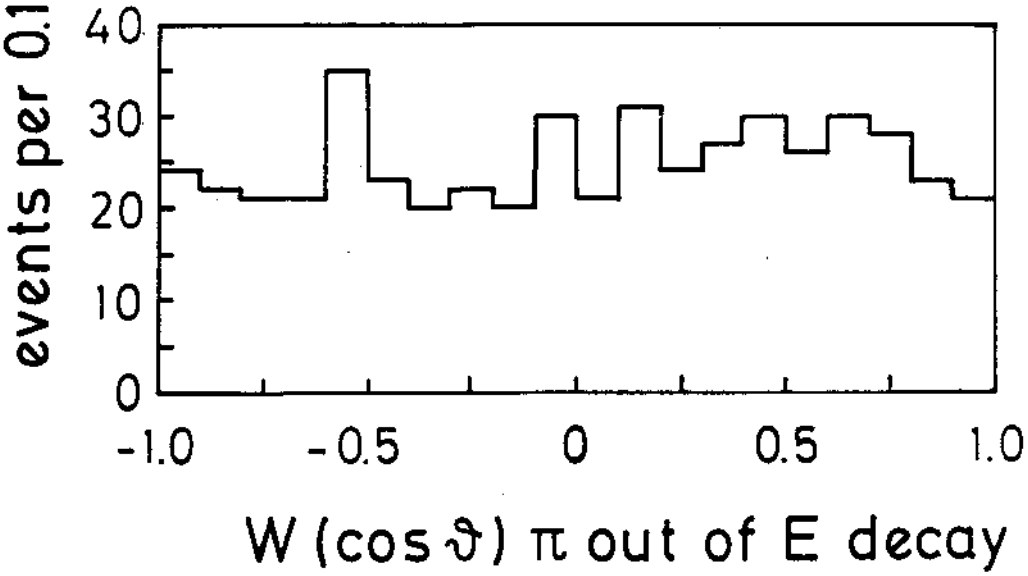
events per 0.1
40
30
20
10
0
-1.0
-0.5
0
0.5
1.0
W (cos ϑ) π out of E decay

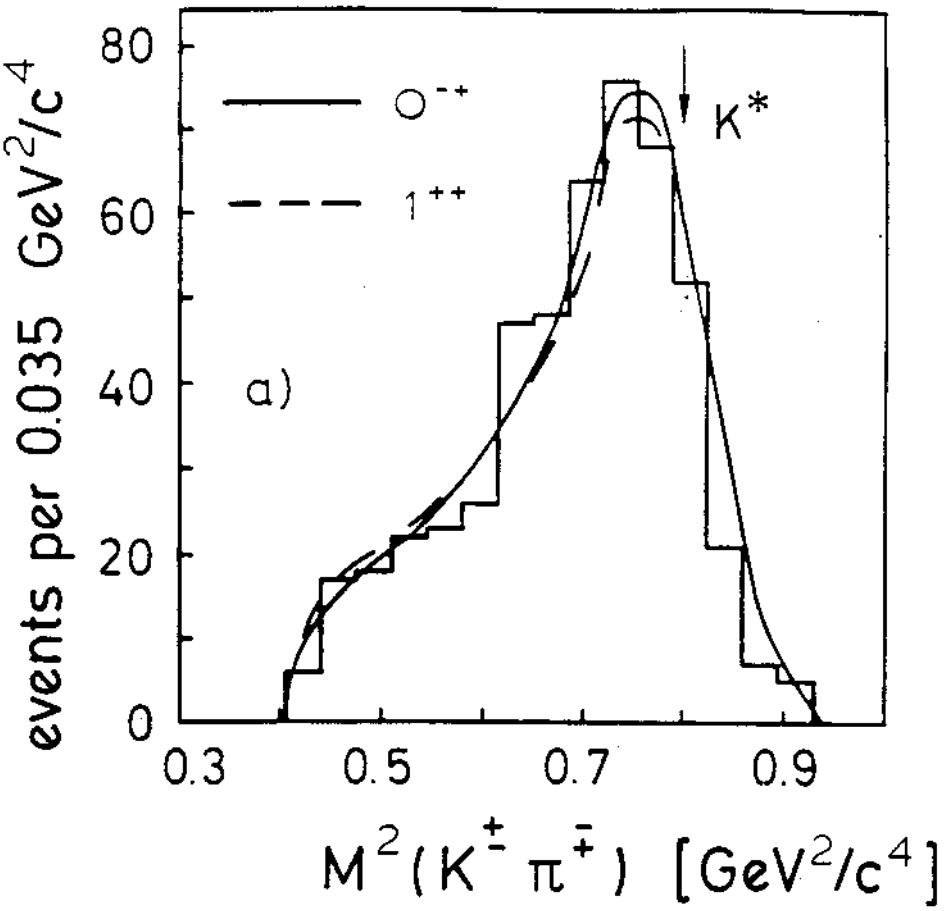
events per 0.035 GeV²/c⁴
80
60
40
20
0
0.3
0.5
0.7
0.9
0⁻⁺
1⁺⁺
K*
a)
M²(K± π∓) [GeV²/c⁴]

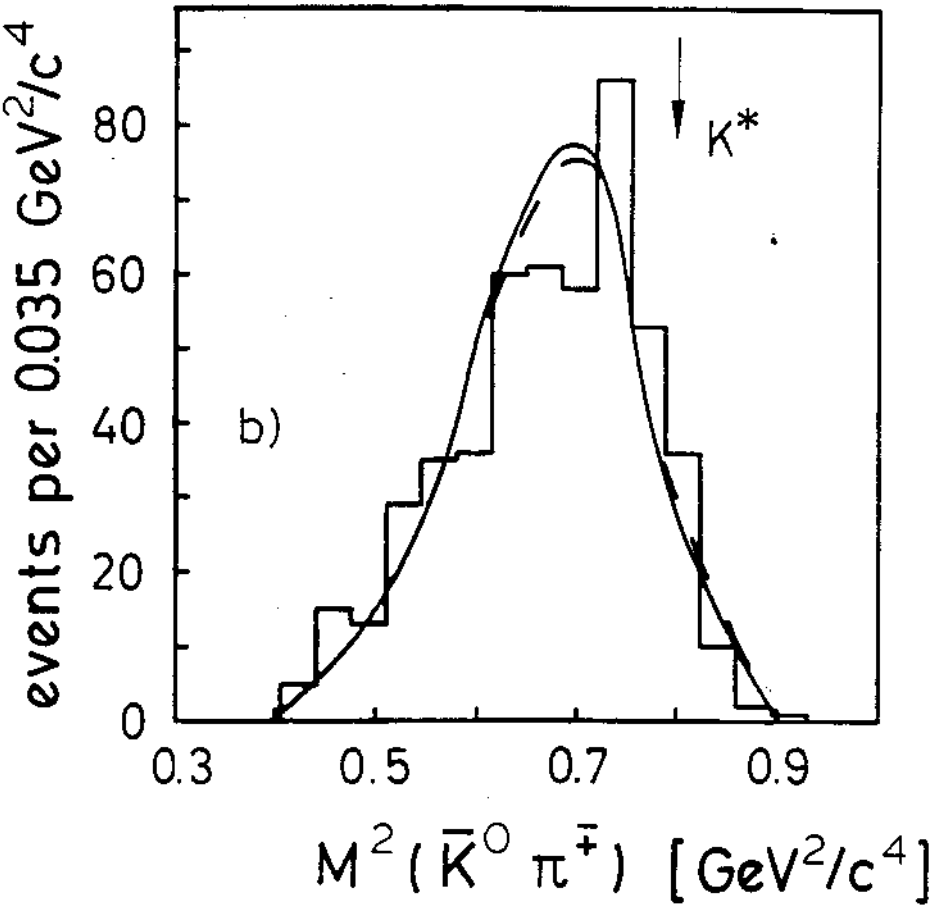
events per 0.035 GeV²/c⁴
80
60
40
20
0
0.3
0.5
0.7
0.9
K*
b)
M²(K̄⁰ π∓) [GeV²/c⁴]

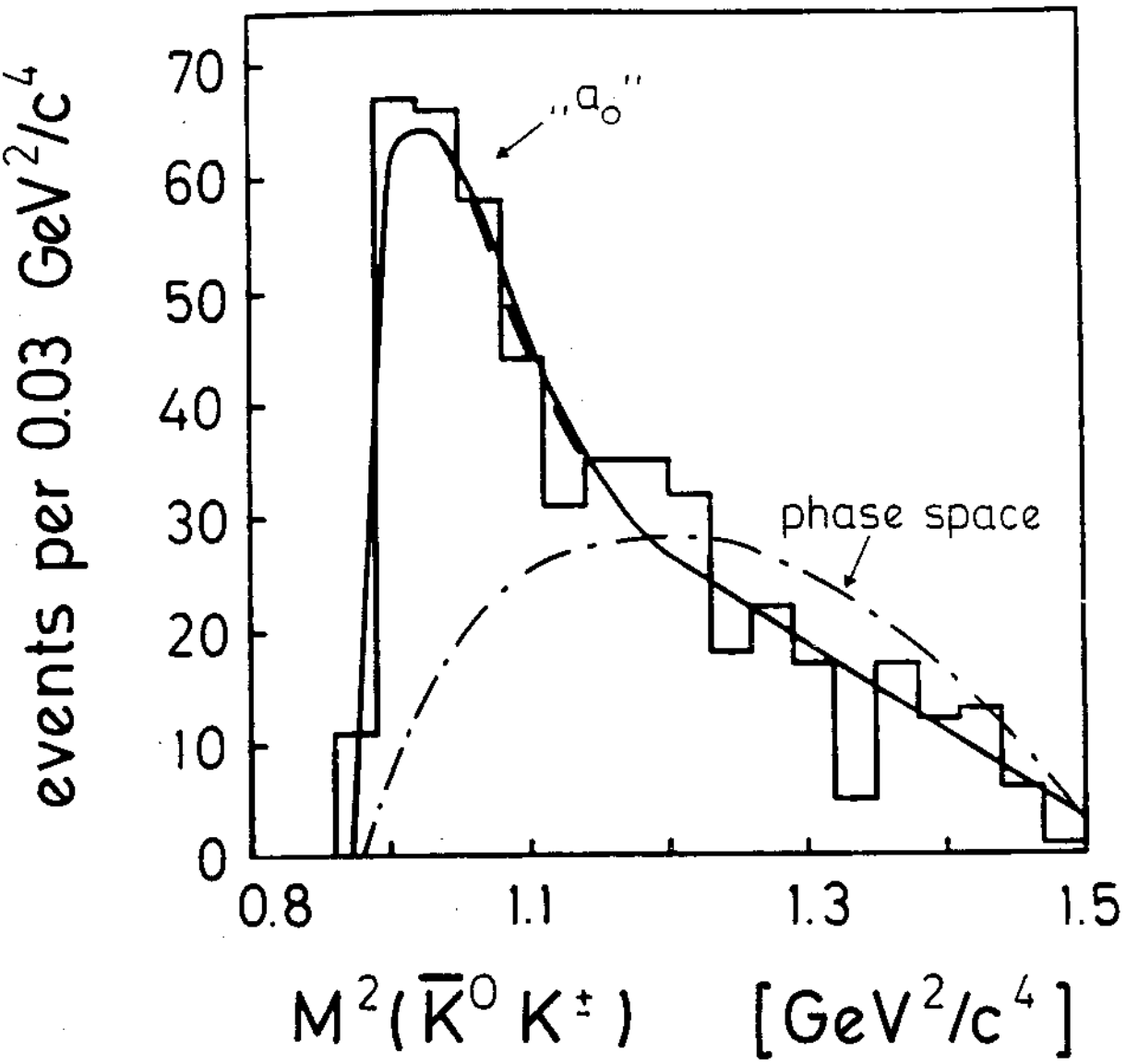
events per 0.03 GeV²/c⁴
70
60
50
40
30
20
10
0
"a₀"
phase space
0.8
1.1
1.3
1.5
M²(K̄⁰ K±) [GeV²/c⁴]

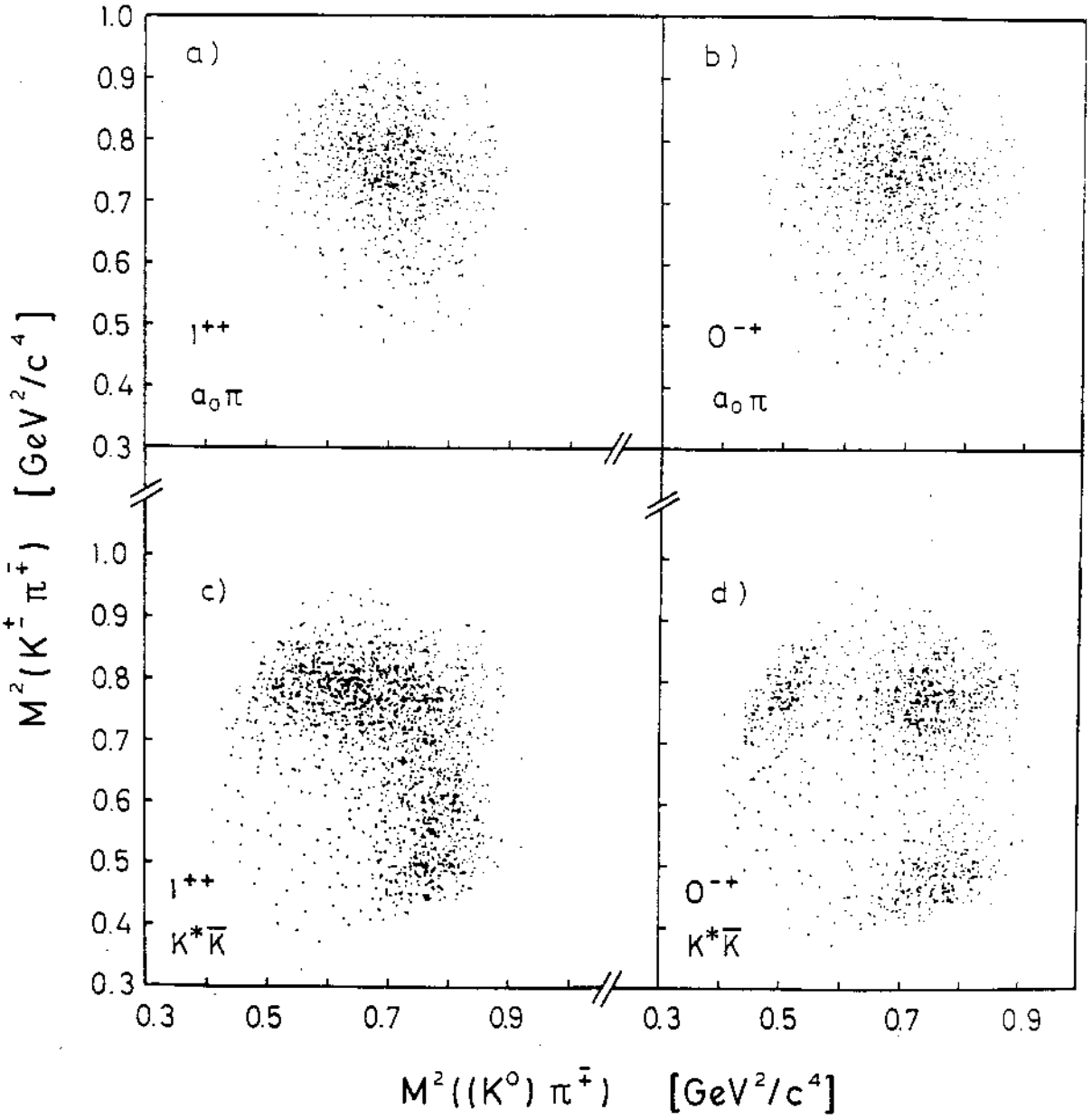
a)
b)
c)
d)
1^{++}
$a_0\pi$
0^{-+}
$a_0\pi$
1^{++}
$K^*\bar{K}$
0^{-+}
$K^*\bar{K}$
$M^2(K^{\pm}\pi^{\mp})$ [GeV^2/c^4]
$M^2((K^0)\pi^{\mp})$ [GeV^2/c^4]
1.0
0.9
0.8
0.7
0.6
0.5
0.4
0.3
0.3
0.5
0.7
0.9

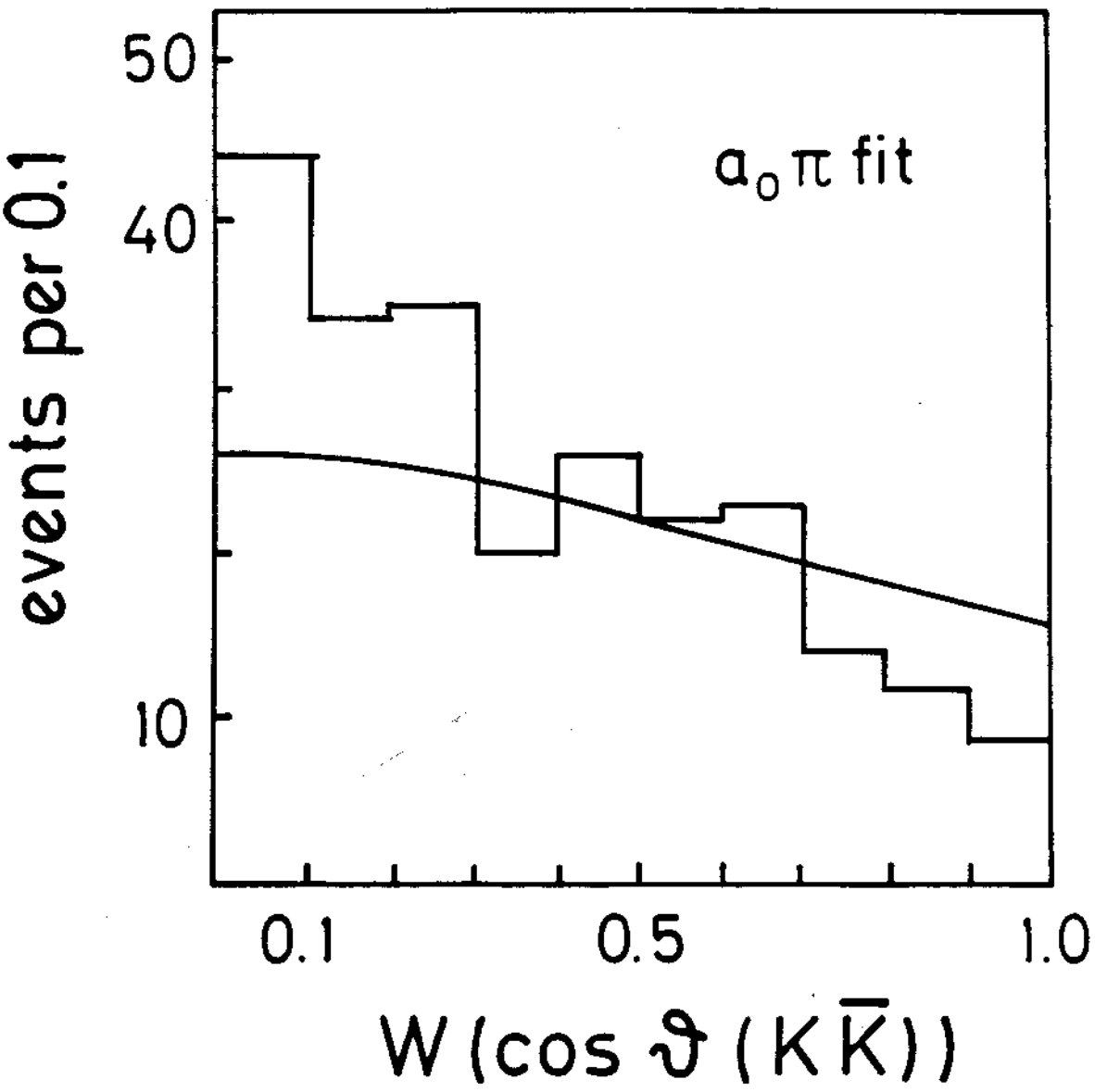
50
40
10
events per 0.1
$a_0\pi$ fit
0.1
0.5
1.0
W (cos ϑ (K K̄))